Available online at www.sciencedirect.com

ScienceDirect

Acta Materialia 89 (2015) 268–277

Acta MATERIALIA

www.elsevier.com/locate/actamat

# Microstructural characteristics and elastic modulus of porous solids

Zhangwei Chen,* Xin Wang, Finn Giuliani and Alan Atkinson

*Department of Materials, Imperial College London, London SW7 2AZ, United Kingdom*

Received 23 November 2014; revised 8 February 2015; accepted 9 February 2015

**Abstract**—Porous $La_{0.6}Sr_{0.4}Co_{0.2}Fe_{0.8}O_{3-\delta}$ ceramic films with different porosities were fabricated by constrained sintering on dense substrates of Gd-doped ceria at 900-1200 °C. The actual digital three dimensional microstructures of the as-sintered films were reconstructed using focused ion beam/scanning electron microscope tomography and their elastic moduli were calculated using finite element modelling based on the reconstructed microstructures. The calculated moduli were found to be in good agreement with experimental results. Porosity was found to be the primary factor influencing the elastic modulus. In order to explore the influence of microstructural features other than porosity the real microstructures, and artificial microstructures based on spherical mono-size particles, were coarsened numerically at constant porosity using a cellular automaton method. The simulation results showed that in the initial stages of sintering, when interparticle necks are small, the modulus increases with the neck size. However, as the coarsening increases further, the modulus becomes insensitive to the details of the microstructure and only depends on porosity. The results also show that simulation gives inaccurate results if the ratio of characteristic length of the simulated volume to the characteristic length of the microstructure is too small (less than approximately a factor of 8).


*Keywords:* Elastic modulus; Porous solid; FIB/SEM tomography; Microstructure; Finite element modelling

## 1. Introduction

The elasticity of porous solids has been extensively studied in the past few decades. Focus has been mainly on the description and prediction of the porosity-dependent mechanical properties such as effective strength, elastic modulus and shear modulus, particularly for ceramic materials prepared by partial sintering of powders. The relationships between elastic modulus and microstructure for partially sintered powders are likely to be quite different from those of similar porous material made by other processing methods (e.g., foams and cellular ceramics) [1,2].

A number of equations, either empirical or semi-empirical, have been proposed to relate elastic properties of porous solids to fractional pore volume. These are based either on fitting experimentally measured data or numerical simulations of ideal regular microstructures. Recently a thorough overview was given by Pabst et al. [3] covering most elastic modulus–porosity relations proposed in the literature and examining the theoretical background and merit of the different relationships. Examples of these commonly used expressions include the linear relationship first developed by Fryxell and Chandler [4] for polycrystalline BeO and a simple exponential relationship proposed by Spriggs [5] for fitting the experimentally measured modulus of porous ceramics. Other non-linear expressions include the Coble–Kingery non-linear relation [1] for solids containing isolated pores, the Phani–Niyogi power-law relation [6,7] to better describe the modulus-porosity data of porous solids over a wide range of porosity and a non-linear relation proposed by Hasselman [8] to ensure that the fitted modulus becomes 0 when porosity reaches 100%. However, most of the relations apply only for narrow ranges of porosity, specific materials or special cases, such as porous materials with a dilute distribution of spherical pores. Furthermore these approaches do not explicitly take into account microstructural parameters other than porosity.

The aim of the present study is to explore how elastic modulus of a typical partially sintered ceramic film depends on its microstructure and whether factors other than porosity have significant influence. This is based on both real 3D microstructures of partially sintered films and artificial microstructures formed from an initial random distribution of uniform mono-size spherical particles. In order to examine microstructure parameters other than porosity, the starting microstructures were coarsened by computer simulation at constant porosity using a cellular automaton (CA) method that mimics mass transport by evaporation and condensation. The elastic properties of the original and coarsened microstructures were then computed using a mechanical FEM simulation and correlated with characteristic quantifiable microstructural features.

The perovskite $La_{0.6}Sr_{0.4}Co_{0.2}Fe_{0.8}O_{3-\delta}$ (LSCF) is a common cathode material used in intermediate temperature solid oxide fuel cells (IT-SOFCs) [9,10] due to its

* Corresponding author.

http://dx.doi.org/10.1016/j.actamat.2015.02.014
1359-6462/

stability, electro-catalytic activity for oxygen reduction, and high electronic and ionic conductivity [11,12]. In this work LSCF films were fabricated by slurry casting followed by sintering at different temperatures ranging from 900 to 1200 °C, resulting in porous films having different pore volume fractions and microstructures. Tomography technique (using either X-ray or FIB/SEM) has emerged over the past few decades as one of the powerful tools for quantitative characterisation and analysis of microstructural and functional properties in many-body physics [13,14]. The actual 3D image based modelling was first made possible largely thanks to the X-ray tomography employed [15,16]. Similarly, the latter FIB/SEM tomography technique allows the 3D reconstruction and analysis of the real spatial microstructures of porous electrodes [17] and has been used in the past to relate their microstructure to electrochemical performance [18–21]. The current study uses this approach to correlate microstructure with elastic mechanical properties.

## 2. Materials and methods

### 2.1. Specimen preparation and characterisation

Porous LSCF films were produced on dense substrates of $Ce_{0.9}Gd_{0.1}O_{1.95}$ (CGO) by slurry casting and sintering at 900, 1000, 1100 or 1200 °C as described previously [22].

The room temperature film-only elastic moduli were determined for the as-sintered porous LSCF films by nanoindentation using a diamond spherical indenter, based on the Oliver–Pharr method [23], and the details are given in [22].

The surface and cross-sectional microstructures of the specimens were studied in 2D using a scanning electron microscope (JSM-5610LV SEM, JEOL, Japan). For 3D characterisation a focused ion beam/scanning electron microscope (FIB/SEM) dual-beam instrument (Helios NanoLab 600i, FEI, USA) was used for sectioning and imaging sequential 2D cross-sectional surface images of the porous specimens. Before FIB sectioning, the specimens were impregnated with low viscosity epoxy resin under vacuum to enhance the grayscale contrast and edge definition between the pore phase and solid phase, and to ensure that the highly porous structures outside the sectioning region remained intact. The so-called "shine-through" effect could also be avoided by the resin impregnation [24]. The specimen was then coated with a thin layer of gold to provide good electronic conductivity and an additional protective platinum layer of 1–2 μm thickness was then deposited on the top surface of the specimen within the FIB/SEM vacuum chamber in order to protect the upper surface and to prevent charging during sectioning and imaging.

A volume of interest (VOI) $20 \times 15 \times 20$ μm was machined for serial sectioning with a cross-shaped fiducial mark to facilitate automatic image registration. Artefacts caused by tilting, drifting and curtaining were manually corrected or minimised by optimising the working parameters [25]. A resolution of 12.5 nm/pixel was used for SEM imaging and thus a 12.5 nm distance was also applied between sectioning of two consecutive images, so that cubic shape voxels were generated. As a result, several hundred 2D images were obtained for each VOI (e.g., Fig. 1(a)).

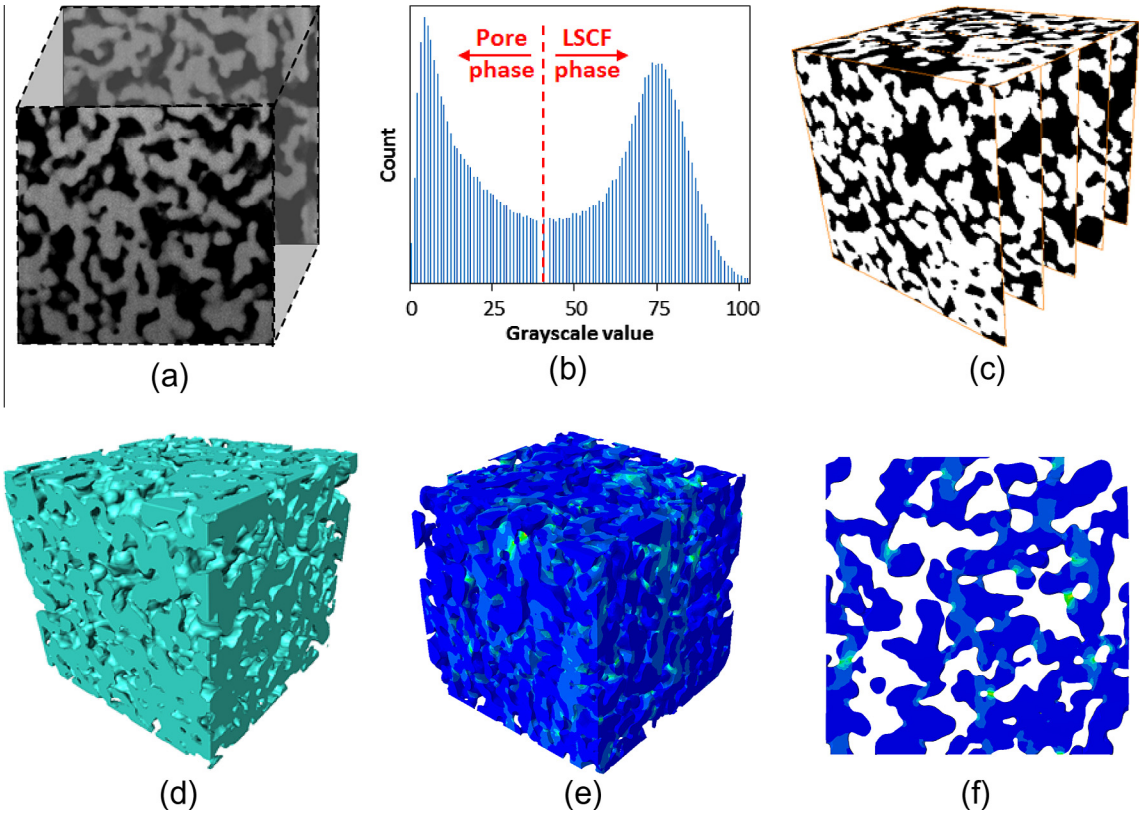


**Fig. 1.** Segmentation and reconstruction: (a) sequential grayscale images acquired, (b) thresholding segmentation based on grayscale histogram, (c) image stack after segmentation (black = pore, white = solid), (d) the reconstructed 3D microstructure generated, (e) 3D stress contour plot of the actual microstructure using FEM and (f) 2D cross-sectional stress contour plot.